Published in final edited form as:
Prog Pediatr Cardiol. 2013 August 1; 35(2): 109–120. doi:10.1016/j.ppedcard.2013.09.002.

Transesophageal Echocardiography in Healthy Young Adult Male Baboons (*Papio hamadryas anubis*): Normal Cardiac Anatomy and Function in Subhuman Primates Compared to Humans

Arthur A. Bert, MD[1,2], **William B. Drake, MD**[2], **Rachael W. Quinn, PhD**[2], **Kathleen M. Brasky, VMD**[3], **James E. O'Brien Jr., MD**[2], **Gary K. Lofland, MD**[2], and **Richard A. Hopkins, MD**[2,*]

[1]Rhode Island/Hasbro Childrens' Hospitals & Miriam Hospital, Warren Alpert School of Medicine at Brown University, Providence, Rhode Island [2]Cardiac Regenerative Surgery Research Laboratories, Cardiology and Cardiac Surgery of The Ward Family Heart Center, Children's Mercy Hospital, Kansas City, Missouri [3]Texas Biomedical Research Institute, San Antonio, Texas

Abstract

Implantable, viable tissue engineered cardiovascular constructs are rapidly approaching clinical translation. Species typically utilized as preclinical large animal models are food stock ungulates for which cross species biological and genomic differences with humans are great. Multiple authorities have recommended developing subhuman primate models for testing regenerative surgical strategies to mitigate xenotransplant inflammation. However, there is a lack of specific quantitative cardiac imaging comparisons between humans and the genomically similar baboons (*Papio hamadryas anubis*). This study was undertaken to translate to baboons transesophageal echocardiographic functional and dimensional criteria defined as necessary for defining cardiac anatomy and function in the perioperative setting. Seventeen young, healthy baboons (approximately 30 kg, similar to 5 year old children) were studied to determine whether the requisite 11 views and 52 measurement parameters could be reliably acquired by transesophageal echocardiography (TEE). The obtained measurements were compared to human adult normative literature values and to a large relational database of pediatric "normal heart" echo measurements. Comparisons to humans, when normalized to BSA, revealed a trend in baboons toward larger mitral and aortic valve effective orifice areas and much larger left ventricular muscle mass and wall thickness, but similar pulmonary and tricuspid valves. By modifying probe positioning relative to human techniques, all recommended TEE views except transgastric could be replicated. To supplement, two transthoracic apical views were discovered that in baboons could reliably replace the transgastric TEE view. Thus, all requisite echo views could be obtained for a complete cardiac evaluation in *Papio hamadryas anubis* to noninvasively quantify cardiac structural anatomy, physiology, and dimensions. Despite similarities between the species, there are subtle and important physiologic and anatomic differences when compared to human.

*Corresponding author: rahopkins@cmh.edu.

Disclosures: The authors and their institutions have no relevant financial disclosures.

Keywords

Heart; Papio; Echocardiography; Transesophageal; Heart Valve Prosthesis; Heart Hypertrophy; Disease Models; Animal; Primate

1.0 Introduction

Surgical implant testing in large animal models has been vital to the development of prosthetic heart valves for clinical use in humans [1]. Chronic animal valve implant survival studies are needed during research and development phases to identify critical design flaws, biological interactions, material failure modes, and technical surgical problems [2]. Such modeling reduces blind alleys and multiple iterations of bench testing while establishing feasibility in realistic surgical settings. Use of large animals for pre-clinical and regulatory implant testing later in the development process can address specific safety and performance issues [3]. Site specific implant testing (orthotopic) is optimal to achieve operating parameters, implant factors, anatomy and physiologic loading conditions that are similar to, or exceed those expected clinically [4]. Various species have been employed, each with specific advantages and disadvantages [5]. Canine, porcine, ovine and bovine models have had specific applicability at various times during the historical development of manufactured cardiovascular devices including mechanical and bioprosthetic valves [6, 7]. The juvenile sheep heart valve chronic implant model has been superior to other species for evaluating crosslinked bioprosthetic valves due to a high propensity for sheep to rapidly (often within 20 weeks) calcify unfavorable biomaterials and are also useful for testing mechanical valves for hydraulic functionality and resistance to thrombosis [8, 9, 10]. This ovine cardiac model appears to recapitulate and predict the primary clinical failure modes, and thus has been the preferred species for first, second, and third generation bioprosthetic valve testing [11, 12, 13].

A new era is beginning in which tissue engineered heart valves are being developed in numerous laboratories around the world [14, 15, 16, 17, 18]. For this new category of valve replacements, failure modes will relate more to cell and matrix biology and to inherent pro-inflammatory characteristics than to traditional design and inert material properties [19, 20]. Because of the over 40 years of use for heart valve preclinical evaluations, the classic ovine model might be considered as a necessary *in vivo* model for cell seeded viable tissue engineered heart valves but may not be optimal or sufficient [21]. There are subtle but important anatomical differences between lower mammalian and primate hearts [22]. The genomic gap from four-legged food stock animals to humans is wide with extremely virulent xenotransplant immune responsivity [23]. The biology of resident multi-potential cells varies between species and differing inflammatory wound healing mechanisms may be critical variables when evaluating tissue engineered heart valve performance [24, 25]. These factors make development of a subhuman primate model for regenerative cardiac valve evaluations appealing, significant and timely [26, 27]. However, for baboons to be useful, the relevant hemodynamic and cardiac structure/function endpoint measurements need to be qualified as feasible, achievable non-invasively, serially applicable for long term testing, applicable during surgical procedures and comparable to clinical measurements in humans [28, 29, 30, 22, 31, 32].

Transthoracic echocardiography has become the standard technology for evaluating chronic cardiac valve performance while transesophageal is the procedure of choice during cardiac surgery and when very precise measurements are needed [33, 34]. By minimizing intervening tissue between the source of the ultrasound waves and the structures of the heart, the transesophageal approach produces optimal images for quantitative measurements,

especially in the evaluation of prosthetic heart valves where acoustic shadowing from highly reflective non-biologic material obscures far-field structures. Guidelines for the evaluation of prosthetic heart valves are specific and extensively validated for valves in the mitral and aortic positions [30]. By comparison, the testing paradigms and quantitative hemodynamic criteria are less well developed for valved conduits, pulmonary valve (PV) replacements, and pediatric valves [35]. Review of the literature reveals only limited use of echocardiography to evaluate cardiac performance in various subhuman primates with an emphasis on transthoracic imaging [15, 23, 36, 37, 29, 22, 31]. For old-world monkeys, the literature emphasis has been macaques rather than baboons [38, 39]. Given that baboons are a better size for intracardiac survival surgery models than macaques, this study was performed to define the utility of transesophageal echocardiography in baboons, to develop reproducible techniques for acquiring the necessary images, to evaluate species specific cardiac anatomy, ventricular and valve performance in young adult *Papio hamadryas anubis* as compared with analogous images, dimensional and functional data in humans. If the baboon becomes a frequently employed cardiac regenerative model, then the generation of more extensive normative reference baboon cardiac dimensions and hemodynamic physiologic values will be important. Finally, since organ allometric scaling is challenging across species, we compared these normative baboon data to both established literature valves for adult normal ranges and also to our own extensive pediatric echocardiographic database to define relevance to children of similar body size and/or to adult physiology [40].

Materials and Methods

Seventeen post-pubescent male baboons (*Papio hamadryas anubis*, age 10.50 ± 0.62; weight 23.2 to 36.2 kg) underwent comprehensive transesophageal echocardiography (TEE) examination. Nine had no subsequent procedures, while eight animals underwent the study prior to use as chronic surgical models [41]. All reported studies were obtained after the first author had acquired sufficient expertise with echocardiography in this species by previously completing over 50 targeted perioperative TEE examinations. Animals were fasted overnight but had access to fluids ad lib until four hours prior to procedures. Normal saline with 5% dextrose was infused intravenously at 125 ml/hour during the procedure to maintain normal intravascular volumes.

Anesthesia protocol

The innate aggressiveness of baboons necessitates deep sedation to provide gentle and safe handling of the animals when removed from their cages, thus these exams establish “resting” values. Prior to TEE examination, animals were sedated with an intramuscular injection of ketamine (6 to 10 mg/kg) and glycopyrrolate (0.02 mg/kg). After establishment of peripheral intravenous access, endotracheal intubation was performed. General anesthesia was maintained with inhalation of isoflurane at 1.5 to 2.0% on controlled ventilation. Some animals received fentanyl boluses (1 to 2 mcg/kg), if their vital signs appeared to indicate excessive sympathetic output. Studies were performed with IACUC approval and in accordance with the Guide for the Care and Use of Laboratory Animals, Eighth Edition (National Research Council, National Academic Press, Washington, DC, 2011) and The Animal Welfare Act of 1976 amendments to the Animal Welfare Act (P.L. 94-279).

Transesophageal echocardiography

Cardiac anatomic structural dimensions, qualitative and quantitative analysis of valves and ventricular function were evaluated by transesophageal echocardiography. A 5.0/3.7 MHz omni-plane transesophageal HP probe was passed into the esophagus after the animal was under general anesthesia. Images were captured in real time on a HP SONOS 2500 platform (Philips Medical Systems) and recorded on videotape for off-line analysis. Baboons were

placed in the supine position during the TEE exams as would be done during median sternotomy surgery.

TEE imaging views

Utilizing the joint American Society of Echocardiography and Society of Cardiovascular Anesthesiologists published guidelines for performing a comprehensive intraoperative multiplane TEE examination as a guide to the template of what constitutes a “complete cardiac exam”, we recorded the modifications in techniques necessary to achieve this goal as a guide for researchers using this species [34]. The goal was to accomplish all 52 critical measurements from the 11 standard recommended clinical TEE imaging views that should be used clinically to evaluate semilunar valve function and the consequential cardiac physiology. We specifically emphasized the standard views most relevant for our semilunar valve tissue engineering research where imaging and quantification of hemodynamic performance of the pulmonary valve (PV) and aortic valves (AV) are vital [42, 43]. Achievement of the following imaging view was deemed critical to a complete evaluation: the mid-esophageal AV short-axis view (ME AVSAX), the midesophageal right ventricular inflow-outflow view (ME RVIO), the midesophageal AV long-axis view (ME AVLAX); the midesophageal four-chamber view (ME4C); the mid esophageal two-chamber view (ME2C); the midesophageal long-axis view (ME LAX); the transgastric (TG) mid papillary left ventricular short-axis view (TGSAX); the TG two-chamber view (TG2C); the TG long-axis view (TGLAX); the deep TG long-axis view (dTGLAX); and the upper esophageal aortic arch short-axis view (UESAX). We suspected that the deep TGLAX view, as well as other TG views might not be reliably obtained in baboons and for which novel substitute views would need to be developed. Similar to humans, there was likely no mid-esophageal imaging plane that would offer an acceptable intercept angle between the vector of blood flow through the LV outflow tract and across the AV to obtain accurate quantitative data. Hence a HP 2.5/2.0 MHz transthoracic ultrasound probe was utilized to ascertain whether transthoracic imaging could obtain supplemental views similar to a classical human transthoracic apical long-axis view, whereby the blood flow out the LVOT and through the AV could be aligned in a near parallel direction with the Doppler beam, thus allowing performance of a “complete” exam.

Anatomic dimensions

All 2D measurements of anatomic dimensions, ventricular function and valvular quantitative data were analyzed off-line. For all cardiac dimensional and ventricular function measurements, at least three separate data points were obtained from different imaging loops and averaged to obtain a final measurement. Measurements of LV wall thickness were made using the short-axis view (SAX) of the LV, or a two-chamber view of the LV (obtained via the transthoracic window, or when available, using the TG view). Both septal and posterior wall thickness were measured at end-diastole. Measurements of RV cavity dimensions were performed from ME two- or four-chamber views, while the LV cavity dimensions were measured from the ME2C view, or from the transthoracic apical view of the LV [38, 44]. The minor axis is taken at the mitral or tricuspid papillary muscle apex level. Each ventricle’s major axis was measured from the mid-plane of the respective atrioventricular valve to the endocardial edge of the chamber apex. All dimensions were measured at end-diastole. End-diastole was defined as the frame with the maximal cavity area in proximity to the start of the QRS complex, while end-systole as the frame with the minimal cavity area in proximity to the end of the T-wave on the ECG.

For measurement of the fractional area change (FAC), the areas of the LV cavity were measured at both end-diastole and systole, from a SAX view of the LV. Quantitative evaluation of LV systolic function was performed by measurement of FAC and/or

calculation of the left ventricular ejection fraction (LVEF) utilizing the modified Simpson's disk summation method [45]. Utilizing the Phillips' software package, the LVEF was calculated with Simpson's method from measurement of LV volumes at end-diastole and systole, by tracing the endocardial borders from well-defined ME2C views of the LV. M-mode of the LV SAX view was one of the modes utilized to determine FAS, but was typically averaged with measurements from 2-dimensional views of the LV SAX as well. LV ejection fraction was determined from the ME2C view of the left ventricle.

Valvular gradients, effective orifice areas, and cardiac outputs

Peak and mean pressure gradients across the native valves were measured by pulsed wave Doppler (PWD). Since most blood flow velocities were less than 100 cm/sec (i.e. 1m/sec) peak PWD seemed to be more accurate especially when multiple angles where utilized with the highest peak value recorded as "peak". When blood flow velocities exceeded 1m/sec, CWD was utilized, or (where appropriate) continuous wave Doppler using the simplified Bernoulli equation. Multiple envelopes were recorded from different imaging windows across the native aortic and pulmonary valves to find those envelopes where blood flow best aligned with the Doppler beam. Peak gradients were the highest recorded, while mean gradients were the average of at least four beats from the imaging window with minimal angulation between the Doppler beam and blood flow direction. PWD imaging was utilized in the RV and LV outflow tracts respectively, with the sample volume icon positioned proximal to the native valve. The RVOT diameter was measured in mid-systole at the site of the PWD sample volume icon in the video loop, since the conical shaped muscular tract changes diameter during the cardiac cycle. The LVOT diameter was best obtained from imaging the LVOT in zoom mode from the ME AVLAX view. Cross sectional areas of each outflow tract were calculated by the equation:

$$\text{Cross sectional area (CSA) of LVOT/RVOT} = \pi \times \left(\frac{\textit{diameter of RVOT or LVOT}}{2}\right)^2$$

Spectral Doppler measurements permit the calculation of cardiac output (CO) for the right ventricle (RV) and left ventricle (LV; RVCO, LVCO), RV and LV stroke volumes (RVSV, LVSV) and, effective orifice area (EOA) by use of the continuity equation:

$$\text{Valve EOA} = (\text{CSA}) \left(\frac{\textit{velocity time interval of outflow tract}}{\textit{velocity time interval across value}}\right)$$

The EOA of the native PV or AV is obtained by placing the respective right or left-sided variables in the equation. To permit indexing of CO, and cardiac dimensions to body surface area (BSA), each animal's BSA was calculated by the Haycock formula [46].

Grading of valvular regurgitation

The presence and severity of regurgitation through native valves were evaluated by color flow Doppler (CFD) imaging. We utilized the American Society of Echocardiography guidelines for evaluating the severity of aortic valvular regurgitation [47]. These guidelines offer little in the way of validated methods to grade severity of pulmonary regurgitation. Therefore, we utilized the following widely employed clinical scale in grading pulmonary regurgitation: trace (CFD regurgitant jet length limited to the immediate valve area and of low velocity), mild (jet length limited to the RVOT, or a jet width:RVOT width ratio of ≤ 30%), moderate (jet extending into right ventricular cavity, or jet width:RVOT width ratio between 31–70%), and severe (jet extending to the tricuspid valve, or jet width:RVOT width ratio ≥ 70% [48]. All echocardiographic images were obtained by a National Board of

Echocardiography certified echocardiographer (AAB) and reviewed independently by another board certified echocardiographer (WBD).

Transthoracic imaging

The inability to obtain deep TG images in the Papio species, combined with limited access to all TG images (especially the TGLAX view), means that baboons do not have a TEE window with adequate alignment of the ultrasound beam to the blood flow out the LVOT and aortic valve. Restricting the examination to only transesophageal views would mean limiting measurements of the AV area to annular diameters and planimetry in the majority of animals. To replace these critical but unobtainable TEE views we sought a complementary transthoracic imaging window for planes useful for spectral Doppler interrogation of both outflow tracts and across aortic and pulmonary valves that is a view equivalent to the human transgastric long axis view (APLAX), as well as an equivalent view of the left ventricular short-axis view (LVSAX).

Statistical analysis

The calculations of means ± standard error, medians and ranges were performed using SPSS (v.17, Chicago, IL) for papio data. Human adult standard reference values are presented as calculated by the original source since such ‘normative’ values are typically presented as broad ranges. Clinical adult data normalization to body mass indices is more commonly used in the context of specific structural disease entities or for prosthetic valve replacement guidelines. To contextualize our measurements in baboons to commonly quoted adult ‘normal’ ranges, we have provided both mean ± standard deviation and the median (range) for our measured data side by side with standard human normal reference ranges. In contrast, pediatric echocardiography data are routinely normalized to BSA/weight/height, simplifying statistical comparisons (*vida infra*). All measurements, images, and findings from all echocardiograms (approximately 1200/month) performed by Children’s Mercy Hospital cardiology are continuously extracted from the Philips Xcelera system and stored in custom Children’s Mercy Hospital Heart Center relational database using a picture archiving and communication system. Subsequent data analysis subroutines have been built to establish normative and pathological data sets by any x-axis factor such as age and BSA from which smooth splines can be fitted for defining and normalizing parameters such as those explored herein. This allows the quantification of percentiles, Z scores, T scores, and Stens. For this normative post-hoc analysis, spline curves were developed using “R,” an open source statistical software (www.r-project.org). Using the R “smooth.spline” function, splines were developed at the 3rd, 10th, 25th, 50th, 75th, 90th, 97th percentiles of compared values: including valve dimensions, ejection fractions, flow velocities, heart rates, left ventricular wall thickness, stroke volumes, and mass indices. In these very large normative data sets, typical parameters of the smooth.spline function could be relaxed, in some cases with the Equivalent Degree of Freedom greater than 100.

Results

Normative TEE measurements in *Papio hamadryas anubis*

Fifty-two classical echo parameters were measured in the subjects defining cardiac structure/function and reported in Table 1. Given the pronounced baboon species sexual dimorphism (males are generally twice the size of females), these initial data were obtained only in males who were relative young (mean 10½ years) and healthy. Perhaps the most striking observation was the great similarity of cardiac orientation, structure, function, and dimensions to human. Hemodynamics during the exams were relatively similar to humans at rest (Table 2). Baboons are generally smaller by weight than the classical 70 kg man and averaged a BSA of 0.83 m^2 versus the human normative reference BSA of 1.86 m^2. Despite

the somatic body mass disparity, the baboon values were typically within the broad population standard ranges for adult human “normals” for structural cardiac dimensions and physiologic variables except for body size, ventricular cavity volumes, semilunar valve orifice dimensions, cardiac output and stroke indices. However, because the cardiac outputs were lower than standard human values, indexing the geometric valve measurements suggested larger effective valve orifice areas.

To establish better somatic size matched cross-species allometric comparisons, the Children’s Mercy Heart Center echocardiography database was mined for normal values across a wide range of BSA, weight, and height to permit graphical representation of expected percentiles for each measurement in a healthy pediatric population in which body size would bracket the test subjects (*Papio hamadryas anubis*). Pediatric normative echocardiographic measurements are typically collected by TTE, as TEE studies are not routinely performed in healthy children for obvious ethical reasons. Using this methodology, size of the left sided valves tended to group around the 90th percentile, whereas the tricuspid approximated the 75th percentile and the PVs were smaller in diameter and generally below the 50th percentile (Figure 1). LVEF was notably low, averaging below the pediatric 3rd percentile (Figure 2) without apparent compensatory elevations in heart rates (Figure 3). However, these baboons are under anesthesia and, by age, are in their adult prime, well after puberty and thus may be more analogous to 20 year old human athletic males for which resting heart rates are closer to 55–60 bpm. The peak flow velocities are similarly low in both the baboon pulmonary artery (PA) and aorta which are parameters typically less affected by age and somatic size beyond infancy. (Figure 4).

Most striking is the LV wall thickness which would be hypertrophic in humans (Figures 5a, 5b) with LV cavity volume encroachment (Figure 5c) and massive LV mass index (Figure 5d) that is even greater when normalized to height (Figure 6). Height has been proposed to better correlate with allometric organ size during growth within and across species [49, 50]. Despite this conspicuous LV hypertrophy, stroke and ejection indices fall within human normal to low-normal ranges (Table 2). LVSV, LVEF, CO and cardiac index are relative lower at rest than similar sized children and thus more analogous to older (albeit on average, larger) human adults (Figure 7) [51].

Methodological comparison of TEE imaging in baboons as compared to human clinical techniques

The requisite eleven TEE and the two supplemental TT views comprising a complete perioperative echocardiography exam in a baboon from which the essential 52 measurement parameters analogous to humans can be assessed are summarized in Table 3. All six of the standard mid-esophageal imaging views could be regularly obtained in the *Papio*, and are similar in cardiac structural orientation to human. For example, the ME SAX view of the AVis ideal for evaluating valve morphology (eg, bicuspid versus tricuspid), and assessing cusp mobility and/or calcification. In systole, planimetry can be used to determine orifice area accurately. Similar to human, we found the ME AVSAX view between 25–45°. A short-axis image adequate for planimetry measurement of the AV orifice area could be obtained in 16 of 17 study animals. The ME AVLAX view reliably images the LVOT, AV, and aortic root, and can be found by rotating the imaging plane to 100- 130° from the ME AVSAX view. This view was useful for measurement of the diameters of the LVOT, AV annulus and ascending aorta, while the application of CFD permitted detection and grading of severity of AV regurgitation. Between these two views, at an imaging plane of 25°–60° we found the ME RVIO view where the right atrium (RA), tricuspid valve, RVOT, PV, and main PA appears to wrap around a short-axis view of the AV. With this view, tricuspid valve gradients could be assessed by PWD, while also detecting and grading the severity of

tricuspid regurgitation by CFD imaging. It is one of two traditional views (the other being the ME RV 2-chamber view), utilized to measure tricuspid valve annulus diameter. Further rotation of both the imaging plane (~80°) and the TEE probe head to the right yielded a mid-esophageal view of the RVOT, PV and proximal PA. This is not a standard human view but in these baboons permitted measurement of the PV annulus and was useful for detecting the presence and severity of pulmonary regurgitation, pulmonic stenosis and subvalvular obstruction with the addition of CFD imaging. While not providing optimal alignment of blood flow direction across the PV and the ultrasound beam, it generated useful assessments of PV gradients.

Further advancement of the TEE probe to the plane revealing the mitral valve (MV) produced the classic ME4C. Analogous to humans, this view demonstrated all four chambers of the heart. However, unlike humans, and despite multiple incremental image plane rotations and retroflexion of the probe head, the ME4C view in *Papio* nearly always foreshortened the left ventricular cavity. While useful for measuring right and left atrium, and RV chamber dimensions, this view did not reliably permit measurement of LV cavity dimensions. It was a useful plane for assessing tricuspid valve function and annulus diameter.

Rotation of the imaging plane to between 60°–90° produces the ME2C, where for both species, the left atrium (LA), MV and LV are all optimally imaged. From this view, left-sided cardiac chamber dimensions were obtained. As in humans, it was the optimal plane to evaluate MV anatomy, physiology, pressure gradients, and detect and grade mitral regurgitation. For baboons, this ME2C view of the LV was clearly the optimal imaging plane to quantify LV systolic performance by calculating biplane LVEF (Simpson's method).

As in humans, rotation of the TEE probe from the ME2C imaging plane to 110°–120° resulted in the ME LAX where the left ventricle inflow and outflow tracts would typically be seen. This was another useful view for evaluation of MV physiology with spectral and CFD imaging, LVOT diameter and blood flow assessment as well as regional LV wall motion (anteroseptal and inferolateral walls). From this position, rotation of the probe to the right with retroflexion reliably produced a useful non-standard (in humans) mid-esophageal view of the right-sided cardiac structures (ME RV2C). This imaging plane was especially useful for right heart chamber dimension measurements, tricuspid valve imaging and Doppler interrogation of the MV.

Advancement of the probe into the stomach with anteflexion produces TG views in humans. Unlike the similar baboon-human mid-esophageal imagery planes, the TG images could not be reliably obtained in the baboon, and in particular deep TG images of the heart could not be obtained in any study animal; all imaging was obstructed by liver parenchyma. Some animals idiosyncratically have a small imaging window between the lobes of the liver that permits a short-axis peek of the right and left ventricles, analogous to the standard TG mid-papillary short-axis view (TGSAX) in humans. This view is ideal for assessment of ventricular wall motion, LV volume, measurement of LV and RV wall thickness, and quantification of LV systolic function by the FAC methodology, yet only three of the 17 study animals yielded such TGSAX views. If the TGSAX view is obtained, rotation of the imaging plane to between 90–100° yields the TG2C view analogous to humans. This imaging plane typically provides a long-axis view of the left ventricle, MV, and its support structures, and the LA. In baboons, this view could be obtained in only the same three animals that yielded useful TGSAX views. When available, as in these same animals, further rotation combined with probe head anteflexion, resulted in a TGLAX view from which spectral Doppler evaluations of blood flow velocities in the LVOT, across the AV and

calculations of pressure gradients across the native left-sided structures and ventricular COs could be reliably measured.

Another TEE view utilized in humans to provide for accurate Doppler interrogation of LVOT and AV blood flow is the deep TGLAX view. No study animal yielded a useful deep TG image, due to the intervening liver parenchyma placing the cardiac structures beyond the imaging field. Finally, withdrawing the TEE probe into the upper esophagus, to the level of the ascending aorta, at an imaging plane of 0°, and rotating the probe head to the right, provided the baboon equivalent view of the UESAX standard view in humans. From this position, rotation of the imaging plane to 40°–80° was needed to image the main PA and PV in an orientation where the direction of blood flow through these structures aligns parallel to the ultrasound beam. In baboons in the UESAX view, the aortic arch is at an oblique axis. This useful view was obtained regularly (13 of 17 animals) in *Papio*, and proved to be a critically important view for measurements of pulmonary valve pressure gradients.

Transthoracic echocardiography

In comparison to humans, intercostal spaces are wider in adult baboons, permitting avoidance of the bony ribs obscuring cardiac structures. Unfortunately, we found that, for the most part, lung parenchyma obstructs transthoracic imaging of the heart and thus as a single methodology, transthoracic echocardiography was of minimal utility. However, a single reliable window for transthoracic imaging was found, usually just to the left of the sternum at the sixth intercostal space. With the echo probe head oriented transversely with a slight cephalad angulation, short-axis views of the right and left ventricles were obtained (LVSAX). These were comparable in utility to the human TGSAX images obtained by TEE, and were usually obtainable (14 of 17 animals). More importantly, we discovered that with this unique approach, an apical long axis (APLAX) view in the baboon is equivalent to a transthoracic apical 5 chamber view. Rotating the transducer to a horizontal imaging window with more extreme cephalad angulation, produced images of the left and right outflow tracts and their respective valves oriented ideally for quantification of native aortic valve physiology. These useful views permitting spectral Doppler interrogation across the native AV and PV and could be obtained in the majority (aortic 14 of 17); (pulmonary 12 of 17) of study animals. This location yields the baboon equivalent of the clinically familiar transthoracic apical views.

Discussion

This study confirms the utility of TEE in defining cardiac anatomy, function, and for quantifying cardiac physiology in baboons. With modern transducer design, electrical amplification and display processing, the image quality and dynamic motion of 2D imaging is superb. Imaging frame rates greater than 30 per second are readily achieved in focused near fields, and permit the capture of fine movements like the intermediate positions of valve cusps. Axial resolution, the ability to delineate two separate objects that lie in the path of the ultrasound beam axis, is optimized with high- frequency transducers. Due to its proximity to the heart, TEE transducers image with frequencies of 2.5 to 7.5 MHz, resulting in axial resolution of approximately 1.5 times the wavelength, or between 0.3 and 0.9mm. Despite technologic improvements, transthoracic 2D image quality can be more variable, primarily due to the increased distance between transducer and the heart, with intervening tissues of high (bone) and low (lung) acoustic impedance. TEE imaging benefits from more consistent image quality due to proximity of the cardiac structures and minimal attenuation of ultrasound signals through mediastinal tissues. These limitations are even more apparent in baboons.

We confirmed that transesophageal echocardiography could be performed with the imaging planes anatomically appropriate in baboons. However, this study also demonstrated that TG views, regularly acquired in humans, are not reliably acquired in this species. In addition, a useful deep TG TEE view could never be obtained. The importance of this finding echocardiographically is that the TGLAX and deep TGLAX views are the only TEE imaging planes that optimally align the Doppler ultrasound beam nearly parallel with the direction of blood flow across the aortic valve, providing the most accurate quantification of valve gradients and blood flow physiology. Baboons have a large liver that regularly occupies the entire cephalad portion of the abdominal cavity, extending well across the midline because of its well-developed left lobe [52]. The stomach is longitudinally oriented along the caudal margin of the liver. This anatomy places liver parenchyma between a TEE probe in the stomach and the cardiac structures, obstructing TG imaging. In a minority of animals there was a small imaging window between the lobes of the liver that did permit a TEE view aligning the LVOT and aortic valve blood flow with the ultrasound beam. Thus only in a minority of animals could TEE imaging alone provide a complete qualitative and quantitative evaluation.

TEE imaging does provide multiple useful views of the PV. Two views are especially useful for adequate alignment of blood flow across the valve. Using spectral Doppler blood flow velocity equation, the modified ME RVIO, and the upper esophageal imaging plane (modified UESAX View) provide excellent alignment of the blood flow across the PV with the ultrasound beam to accurately quantify valve gradients. This is a critical imaging window for evaluation of PV conduits frequently used in pediatric cardiac repairs.

Unlike in the far smaller rhesus macaque, transthoracic echocardiography is overall of limited utility in baboons due to obscuration by lung tissue, but two views were discovered to make critical supplemental contributions to the TEE exam. In *Papio*, the apex of the heart lies to the left of the sternum at the level of the sixth intercostal space. Placing the transthoracic probe near this parasternal position with cranial angulation regularly produced an image analogous to the APLAX in the human that was ideal for Doppler interrogation of the blood flow across the native aortic valve, and in many cases with small rightward probe angulation across the native PV as well. The addition of these two transthoracic views made possible a ‘complete’ echocardiographic evaluation of all study animals as defined by the American Society of Echocardiography [34].

Subhuman primates as cardiovascular structure/function models

When considering the baboon as a model for preclinical cardiac research, and utilizing TEE measurements as critical dependent parameters careful consideration of the data in the figures and tables is mandatory. However, the values in human normal adult standard tables typically encompass such a broad range as to make rigorous comparisons difficult. Nevertheless, left ventricular mass measurements in baboons are clearly elevated and would be considered pathological LV hypertrophy in humans (Figures 5 and 6) [53, 49, 54]. Among the other intra-cardiac anatomical measurements, the proportionately larger effective orifice areas of the systemic valves (mitral and aortic) in baboons were notable. Teleologically, the larger mitral orifice would reduce resistance to increased LV in-flow during acutely increased systemic CO achieved by all mechanisms including enhanced contractility, volume preload augmentation and/or sudden heart rate elevations. Similarly, the aortic annulus would be functionally minimally restrictive as reflected by the low measured gradients. During these studies, and our experience with cardiopulmonary bypass supported cardiac surgery in baboons, we noted that the baboon has five additional features of their cardiovascular system that appear to optimize this species for sudden bursts of maximal exertion that would be best supported by acute massive increases in CO and central

blood pressures for enhanced oxygenated blood delivery to muscle capillary beds: 1) an enhanced LV mass; 2) low pulmonary vascular resistance; 3) a muscularized mechanism of spleno-splanchnic blood volume reserve available for acute auto-transfusion augmentation of circulatory blood volume; 4) thicker PA, aortic and systemic peripheral vessel walls suggesting enhanced vascular wall muscularity and tone; 5) a very large left coronary artery system with a huge left main coronary orifice that would reduce geometric Poiseuille resistance to large acute increases in blood flow to a highly muscularized LV [41]. In contrast, the right coronary artery is comparatively miniscule as further evidence of a systemic ventricle dominant heart. The thicker vessel wall dimensions extend at least to the femoral arteries and veins suggesting the substrate for hypercontractile vasomotor activity in both the distributive and capacitance vessels that would facilitate sudden blood volume shifts.

Normative adult human transesophageal echocardiographic measurements of intracardiac dimensions have demonstrated significant proportionality to BSA for most values, however, the relationship is not strictly linear nor necessarily similar for different anatomical structures (e.g. aortic valve diameter, LV volume, etc.) [55, 56]. Despite nonlinearity, somatic size is a dominant factor in cardiac dimensions. For example, after indexing to BSA, in humans, other factors such as gender rarely have clinically significant independent effects [57]. Thus, both absolute values and BSA indexed measurements should be reported when echocardiography is used to measure experimental effects. Allometric scaling of anatomical structural dimensions across species is an important and challenging problem [58]. In cardiac surgery, the calculation of expected cardiac outputs to predict adequate cardiopulmonary bypass flow rates has rested on the concept that baseline/resting nutrient needs (specifically oxygen) are proportional to metabolic rates which are roughly proportional to body size (typically calculated in terms of BSA) [59]. Vascular pathways and cardiac structural dimensions are developmentally regulated by magnitude of blood flow prompting comparisons normalizing structures such as valve and vascular areas to BSA. There is controversy as to the degree of linearity and the theoretical, optimal and actually observed exponential relationships of valve areas to body size. Estimates vary between $BSA^{0.5}$ to $BSA^{1.0}$ To add to the complexity, numerous equations for calculating BSA in humans and subhuman species have been formulated. We chose the Haycock formula for calculating BSA as it has been found to be one of the better predictors in children, likely due to inherent modest devaluation of lower extremity contribution to metabolic needs which likely also applies to upper body dominant baboons [46]. Also, BSA calculations are based on both weight and height. The semi-upright posture of baboons results in hip angulation so crown-rump length is used as a reproducible surrogate measurement for height. The Haycock equation produces similar values to other frequently used pediatric clinical formulae such as the Mosteller and DuBois. Using the Haycock BSA, the indexed value measurements, in our study population appear to scale relatively similarly to human (noting the trend shifts previously indentified) and normalize the measurements in a useful and predictable fashion [60, 61]. For example, the abnormally elevated indexed ventricular mass measurements appear to accurately reflect the baboon qualitative anatomy.

In addition to limited subject numbers, this study has other limitations. In these anesthetized baboons, baseline catecholamine blood levels are likely lower than in awake states. In other experimental surgery studies, we have found it feasible to add to the baseline resting echocardiography exams stepped dobutamine stress echocardiography (data not reported here) in both sheep and baboons to evaluate latent valve or cardiac dysfunction as recommended clinically [62]. Due to somatic size dimorphism, these TEE data were obtained only in healthy young males and thus may not be representative of female gender even with indexing to body size. The anthropometric measurements for these baboons are similar to 5 year old North American children, but the cardiovascular physiology appears to

reflect post-pubescent adults. The thick arterial walls with decreased lumen to external diameter ratio may render this species unsuitable for testing of catheter based technologies requiring systemic access.

This work has revealed a number of important findings. First, we have demonstrated that by relying primarily on transesophageal views, supplemented with two unique baboon-specific parasternal transthoracic apical views obtained with a single probe position, echocardiography provides a comprehensive evaluation for noninvasively quantifying baboon cardiac structural anatomy, physiology, and dimensions that can be easily compared to standard clinical human data. Second, the *Papio* heart is structurally and quantitatively similar to human with specific exceptions of elevated LV wall mass, thickened vessel walls (PA and aorta), and oversized MV orifice dimensions.

Finally, by following the developed methodological guidelines, cardiac TEE imaging in baboons provides an excellent method for intraoperative and serial non-invasive *in vivo* evaluation of cardiac anatomy and physiology to model cardiovascular diseases and to evaluate drug and device therapies. It is specifically relevant to preclinical evaluation of tissue engineered semilunar heart valves for children as both pulmonary and the aortic valves and outflow tracts could be meticulously evaluated. By providing very specific technical procedures as described, standardization and comparability across researchers is attainable as in clinical methodologies. As a subhuman primate species, the baboon may be a helpful addition to the traditional *ungulate* models for preclinical testing of a range of viable tissue engineered cardiovascular constructs.

Acknowledgments

This work was supported in part by NIH Grant #P51RR013986-11.

References

1. Barnhart GR, Jones M, Ishihara T, Chavez AM, Rose DM, Ferrans VJ. Bioprosthetic valvular failure. Clinical and pathological observations in an experimental animal model. J Thorac Cardiovasc Surg. 1982; 83:618–31. [PubMed: 7062773]
2. Gallegos RP, Nockel PJ, Rivard AL, Bianco RW. The current state of *in-vivo* pre-clinical animal models for heart valve evaluation. J Heart Valve Dis. 2005; 14:423–32. [PubMed: 15974538]
3. Grehan JF, Casagrande I, Oliveira EL, et al. A juvenile sheep model for the long-term evaluation of stentless bioprostheses implanted as aortic root replacements. J Heart Valve Dis. 2001; 10:505–12. [PubMed: 11499598]
4. Salerno CT, Droel J, Bianco RW. Current state of *in vivo* preclinical heart valve evaluation. J Heart Valve Dis. 1998; 7:158–62. [PubMed: 9587855]
5. Neethling W, Hodge A, Glancy R. Kangaroo versus Freestyle® stentless bioprostheses in a juvenile sheep model: hemodynamic performance and calcification behavior. J Card Surg. 2005; 20:29–34. [PubMed: 15673407]
6. Roosens B, Bala G, Droogmans S, Van Camp G, Breyne J, Cosyns B. Animal models of organic heart valve disease. Int J Cardiol. 2013; 165:398–409. [PubMed: 22475840]
7. Ouyang DW, Salerno CT, Pederson TS, Bolman RM 3rd, Bianco RW. Long-term evaluation of orthotopically implanted stentless bioprosthetic aortic valves in juvenile sheep. J Invest Surg. 1998; 11:175–83. [PubMed: 9743485]
8. Flameng W, Jashari R, De Visscher G, Mesure L, Meuris B. Calcification of allograft and stentless xenograft valves for right ventricular outflow tract reconstruction: an experimental study in adolescent sheep. J Thorac Cardiovasc Surg. 2011; 141:1513–21. [PubMed: 21093875]
9. Hopkins RA, Jones AL, Wolfinbarger L, Moore MA, Bert AA, Lofland GK. Decellularization reduces calcification while improving both durability and 1-year functional results of pulmonary

homograft valves in juvenile sheep. J Thorac Cardiovasc Surg. 2009; 137:907–13. [PubMed: 19327516]

10. Salerno CT, Pederson TS, Ouyang DW, Bolman RM 3rd, Bianco RW. Chronic evaluation of orthotopically implanted bileaflet mechanical aortic valves in adult domestic sheep. J Invest Surg. 1998; 11:341–47. [PubMed: 9827651]
11. David TE. Aortic valve replacement with stentless porcine bioprostheses. J Card Surg. 1998; 13:344–51. [PubMed: 10440649]
12. Sacks MS, Yoganathan AP. Heart valve function: a biomechanical perspective. Philos Trans R Soc Lond B Biol Sci. 2007; 362:1369–91. [PubMed: 17588873]
13. Schoen FJ, Levy RJ, Hilbert SL, Bianco RW. Antimineralization treatments for bioprosthetic heart valves. Assessment of efficacy and safety. J Thorac Cardiovasc Surg. 1992; 104:1285–88. [PubMed: 1434707]
14. Brody S, Pandit A. Approaches to heart valve tissue engineering scaffold design. J Biomed Mater Res B Appl Biomater. 2007; 83:16–43. [PubMed: 17318822]
15. Hjortnaes J, Bouten CV, Van Herwerden LA, Grundeman PF, Kluin J. Translating autologous heart valve tissue engineering from bench to bed. Tissue Eng Part B. 2009; 15:307–17.
16. Hopkins R. Cardiac surgeon's primer: tissue-engineered cardiac valves. Semin Thorac Cardiovasc Surg Ped Card Surg Annu. 2007; 10:125–35.
17. Dean EW, Udelsman B, Breuer CK. Current advances in the translation of vascular tissue engineering to the treatment of pediatric congenital heart disease. Yale J of Bio & Med. 2012; 85:229–38. [PubMed: 22737051]
18. Emmert MY, Weber B, Behr L, et al. Transapical aortic implantation of autologous marrow stromal cell-based tissue-engineered heart valves: First experiences in the systemic circulation. J Am Coll Cardiol Intv. 2011; 4:822–23.
19. Jordan JE, Williams JK, Lee SJ, Raghavan D, Atala A, Yoo JJ. Bioengineered self-seeding heart valves. J Thorac Cardiovasc Surg. 2012; 143:201–08. [PubMed: 22047685]
20. Baraki H, Tudorache I, Braun M, et al. Orthotopic replacement of the aortic valve with decellularized allograft in a sheep model. Biomaterials. 2009; 30:6240–46. [PubMed: 19703713]
21. Dohmen PM, Ozaki S, Yperman J, Flameng W, Konertz W. Lack of calcification of tissue engineered heart valves in juvenile sheep. Semin Thorac Cardiovasc Surg. 2001; 13:93–8. [PubMed: 11805956]
22. Dennis AT, Castro JM, Heffernan S, Hennessy A. Haemodynamics using transthoracic echocardiography in healthy pregnant and non-pregnant baboons (*Papio hamadryas*). J Med Primatol. 2012; 41:122–29. [PubMed: 22272984]
23. Hopkins R, Bert A, Hilbert S, et al. Bioengineered human and allogeneic pulmonary valve conduits chronically implanted orthotopically in baboons: Hemodynamic performance and immunologic consequences. J Thorac Cardiovasc Surg. 2012; 145:1098–1107. [PubMed: 22841171]
24. Asano M, Gundry SR, Izutani H, Cannarella SN, Fagoaga O, Bailey LL. Baboons undergoing orthotopic concordant cardiac xenotransplantation surviving more than 300 days: Effect of immunosuppressive regimen. J Thorac Cardiovasc Surg. 2003; 125:60–70. [PubMed: 12538986]
25. Dagher I, Boudechiche L, Branger J, et al. Efficient hepatocyte engraftment in a nonhuman primate model after partial portal vein embolization. Transplantation. 2006; 82:1067–73. [PubMed: 17060856]
26. Dekant, W.; Testai, E. [Internet]. Opinion on: The need for non-human primates in biomedical research, production and testing of products and devices; SCHER: Scientific Committee on Health and Environmental Risks. 2009. p. 20-21.[Cited 13 May 2013]. Available at: ec.europa.eu/health/ph_risk/committees/04_scher/docs/scher_o_110.pdf
27. Weber B, Scherman J, Emmert MY, et al. Injectable living marrow stromal cell-based autologous tissue engineered heart valves: first experiences with a one-step intervention in primates. Eur Heart J. 2011; 32:2830–40. [PubMed: 21415068]
28. Champion HC, Michelakis ED, Hassoun PM. Comprehensive invasive and noninvasive approach to the right ventricle-pulmonary circulation unit: State of the art and clinical and research implications. Circulation. 2009; 120:992–1007. [PubMed: 19752350]

29. Gottlieb D, Kunal T, Emani S, et al. *In vivo* monitoring of function of autologous engineered pulmonary valve. J Thorac Cardiovasc Surg. 2010; 139:723–31. [PubMed: 20176213]
30. Zoghbi WA, Chambers JB, Dumesnil JG, et al. Recommendations for evaluation of prosthetic valves with echocardiography and doppler ultrasound. J Am Soc Echocardiogr. 2009; 22:975–1014. [PubMed: 19733789]
31. Guenter CA, McCaffree DR, Davis LJ, Smith VS. Hemodynamic characteristics and blood gas exchange in the normal baboon. J Appl Physiology. 1968; 25:507–10.
32. Lee C, Kim YM, Lee C-H, et al. Outcomes of pulmonary valve replacement in 170 patients with chronic pulmonary regurgitation after relief of right ventricular outflow tract obstruction. J Am Coll Cardiol. 2012; 60:1005–14. [PubMed: 22921969]
33. Schiller N, Shah P, Crawford M, et al. American society of echocardiography committee on standards - subcommittee on quantification of two-dimensional echocardiograms. J Am Soc Echocardiogr. 1989; 2:358–67. [PubMed: 2698218]
34. Shanewise J, Cheung A, Aronson S, et al. ASE/SCA guidelines for performing a comprehensive intraoperative multiplane transesophageal echocardiography examination: recommendations of the American Society of Echocardiography Council for Intraoperative Echocardiography and the Society of Cardiovascular Anesthesiologists Task Force for Certification in Perioperative Transesophageal Echocardiography. Anesth Analg. 1999; 89:870–84. [PubMed: 10512257]
35. Otto, C. Textbook of Clinical Echocardiography. 5. Philadelphia: Elsevier; 2012. p. 466-512.
36. Premawardhana U, Hoskins M, Celermajer D. Transvenous echo doppler in baboons: a new window to the cardiovascular system. Clinical Science. 2000; 99:141–47. [PubMed: 10918047]
37. Lehner G, Fischlein T, Baretton G, Murphy JG, Reichart B. Endothelialized biological heart valve prostheses in the non-human primate model. Eur J Cardiothorac Surg. 1997; 11:498–504. [PubMed: 9105815]
38. Lazar JM, Qureshi G, Qureshi MR, et al. Left ventricular systolic and diastolic function in healthy adult bonnet macaques *(Macaca radiata)*. Cardiology. 2009; 113:116–21. [PubMed: 19033721]
39. Kocarz CE, Padrid PA, Shroff SG, Weinert L, Lang RM. Doppler echocardiographic reference values for healthy rhesus monkeys under ketamine hydrochloride sedation. J Med Primatol. 1997; 26:287–98. [PubMed: 9438222]
40. Cohen G, White M, Sochowski R, et al. Reference values for normal adult transesophageal echocardiographic measurements. J Am Soc Echocardiogr. 1995; 8:221–30. [PubMed: 7640014]
41. Whittaker C, Grist G, Bert A, et al. Pediatric cardiopulmonary bypass adaptations for long-term survival of baboons undergoing pulmonary artery replacement. J Extra Corpor Technol. 2010; 42:223–31. [PubMed: 21114226]
42. Quinn RW, Hilbert SL, Bert AA, et al. Performance and morphology of decellularized pulmonary valves implanted in juvenile sheep. Ann Thorac Surg. 2011; 92:131–37. [PubMed: 21718838]
43. Quinn RW, Hilbert SL, Converse GL, et al. Enhanced autologous re-endothelialization of decellularized and extracellular matrix conditioned allografts implanted into the right ventricular outflow tracts of juvenile sheep. Cardiovasc Eng Technol. 2012; 3:217–27.
44. Wahr DW, Wang YS, Schiller NB. Left ventricular volumes determined by two-dimensional echocardiography in a normal adult population. J Am Coll Cardiol. 1983; 1:863–68. [PubMed: 6687472]
45. Teichholz LE, Kreulen T, Herman MV, Gorlin R. Problems in echocardiographic volume determinations: Echocardiographic-angiographic correlations in the presence or absence of asynergy. Am J Cardiol. 1976; 37:7–11. [PubMed: 1244736]
46. Haycock GB, Schwartz GJ, Wisotsky DH. Geometric method for measuring body surface area: a height-weight formula validated in infants, children, and adults. J Pediatr. 1978; 93:62–6. [PubMed: 650346]
47. Zoghbi WA, Enriquez-Sarano M, Foster E, et al. Recommendations for evaluation of the severity of native valvular regurgitation with two-dimensional and doppler echocardiography. J Am Soc Echocardiogr. 2003; 16:777–802. [PubMed: 12835667]
48. Williams RV, Minich LL, Shaddy RE, Pagotto LT, Tani LY. Comparison of doppler echocardiography with angiography for determining the severity of pulmonary regurgitation. Am J of Cardiol. 2002; 89:1438–41. [PubMed: 12062746]

49. de Simone G, Daniels SR, Devereux RB, et al. Left ventricular mass and body size in normotensive children and adults: Assessment of allometric relations and impact of overweight. J Am Coll Cardiol. 1992; 20:1251–60. [PubMed: 1401629]
50. Sluysmans T, Colan SD. Theoretical and empirical derivation of cardiovascular allometric relationships in children. J Appl Physiol. 2005; 99:445–57. [PubMed: 15557009]
51. Kronik G, Slany J, Mosslacher H. Comparative value of eight M-mode echocardiographic formulas for determining left ventricular stroke volume. A correlative study with thermodilution and left ventricular single plane cineangiography. Circulation. 1979; 60:1308–16. [PubMed: 498456]
52. Swindler, DR.; Wood, CD. An Atlas of Primate Gross Anatomy: Baboon, Chimpanzee, and Man. Malabar, FL: Robert E. Krieger Publishing Co; 1982. p. 14-19.
53. Hoit B, Shao Y, Gabel M, Walsh R. Disparate effects of early pressure overload hypertrophy on velocity-dependent and force-dependent indices of ventricular performance in the conscious baboon. Circulation. 1995; 91:1213–20. [PubMed: 7850961]
54. Pearlman JD, Triulzi MO, King ME, Newell J, Weyman AE. Limits of normal left ventricular dimensions in growth and development: analysis of dimensions and variance in the two-dimensional echocardiograms of 268 normal healthy subjects. J Am Coll Cardiol. 1988; 12:1432–41. [PubMed: 3192840]
55. Hopkins, R. Cardiac reconstructions with allograft tissues. New York: Springer Science+Business Media, Inc; 2005. p. 621-622.
56. Capps SB, Elkins RC, Fronk DM. Body surface area as a predictor of aortic and pulmonary valve diameter. J Thorac Cardiovasc Surg. 2000; 119:975–82. [PubMed: 10788818]
57. Verbraecken J, Van de Heyning P, De Backer W, Van Gaal L. Body surface area in normal-weight, overweight, and obese adults. A comparison study. Metabolism. 2006; 55:515–24. [PubMed: 16546483]
58. White CR. Allometric scaling of mammalian metabolism. J Exp Biol. 2005; 208:1611–19. [PubMed: 15855392]
59. Blinman T, Cook R. Allometric prediction of energy expenditure in infants and children. ICAN: Infant, Child, & Adolescent Nutrition. 2011; 3:216–24.
60. Gardin JM, Burn CS, Childs WJ, Henry WL. Evaluation of blood flow velocity in the ascending aorta and main pulmonary artery of normal subjects by Doppler echocardiography. Am Heart J. 1984; 107:310–19. [PubMed: 6695664]
61. Lang RM, Bierig M, Devereux RB, et al. Recommendations for chamber quantification. Eur J Echocardiogr. 2006; 7:79–108. [PubMed: 16458610]
62. Pibarot P, Dumesnil JG, Jobin J, Cartier P, Honos G, Durand L-G. Hemodynamic and physical performance during maximal exercise in patients with an aortic bioprosthetic valve : Comparison of stentless versus stented bioprostheses. J Am Coll Card. 1999; 34:1609–17.
63. Tamas E, Nylander E. Echocardiographic description of the anatomic relations within the normal aortic root. J Heart Valve Dis. 2007; 16:240–46. [PubMed: 17578042]
64. Troy BL, Pombo J, Rackley CE. Measurement of left ventricular wall thickness and mass by echocardiography. Circulation. 1972; 45:602–11. [PubMed: 4258936]

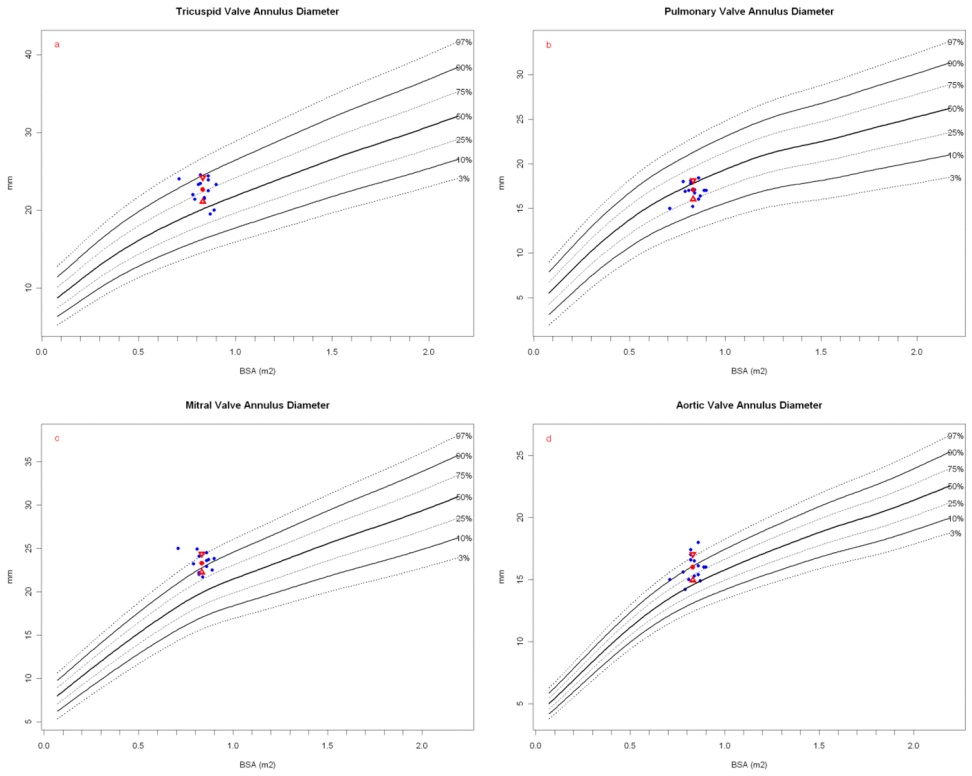

Figure 1.

Valve diameters at the annulus. *Papio* measurements (blue dots) are plotted against a measured normal human cohort model. *Papio* mean (red dot) and standard deviation (red triangles) are shown. The number of normal human measurements used in the reference model is shown as "N=". (a) *Papio* tricuspid valve annulus plotted on human normal model (N = 1353) and (b) *Papio* PV annulus plotted on normal human model (N = 1097). Both the tricuspid valve and PV measurements are within the expected range for humans of similar BSA. Both the (c) *Papio* MV annulus plotted on human normal model (N = 1164) and (d) *Papio* AV annulus plotted on human normal model (N = 1210) dimensions are consistently at the upper normal range for human, with the *Papio* mean around the 90th percentile for humans for both valves.

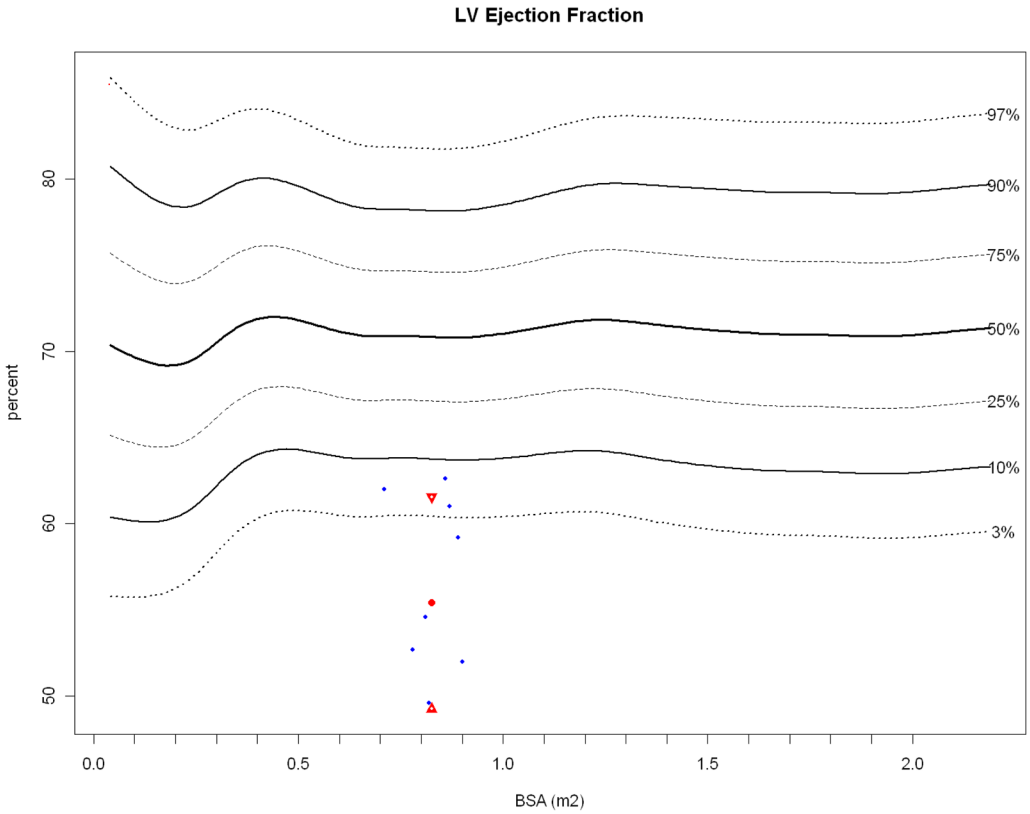

Figure 2.

Papio LVEF (blue dots, obtained while under anesthesia) plotted against normal resting human LVEF (N = 14,261) obtained during transthoracic echocardiography, with the *Papio* mean (red dot) and standard deviation (red triangles). As with heart rate, general anesthesia may have depressed LV contractility.

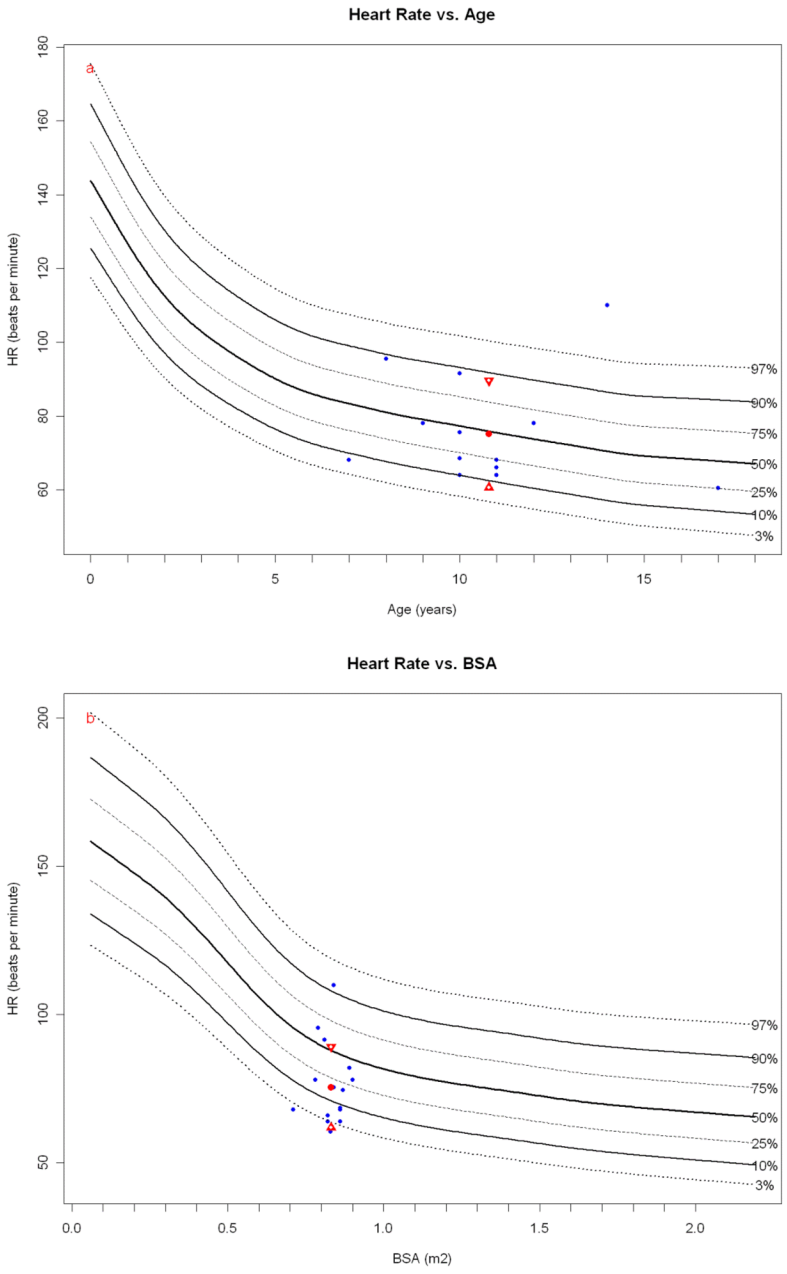

Figure 3.

Papio heart rate (obtained while under anesthesia) plotted against resting human heart rate normals obtained during transthoracic echocardiography (blue dots). The *Papio* mean (red dot) and standard deviation (red triangles) are shown. While the heart rates are obtained in slightly different physiologic states in each species, it is interesting to note that the age-based *Papio* heart rate compares more favorably to the human than the BSA-based heart rate.

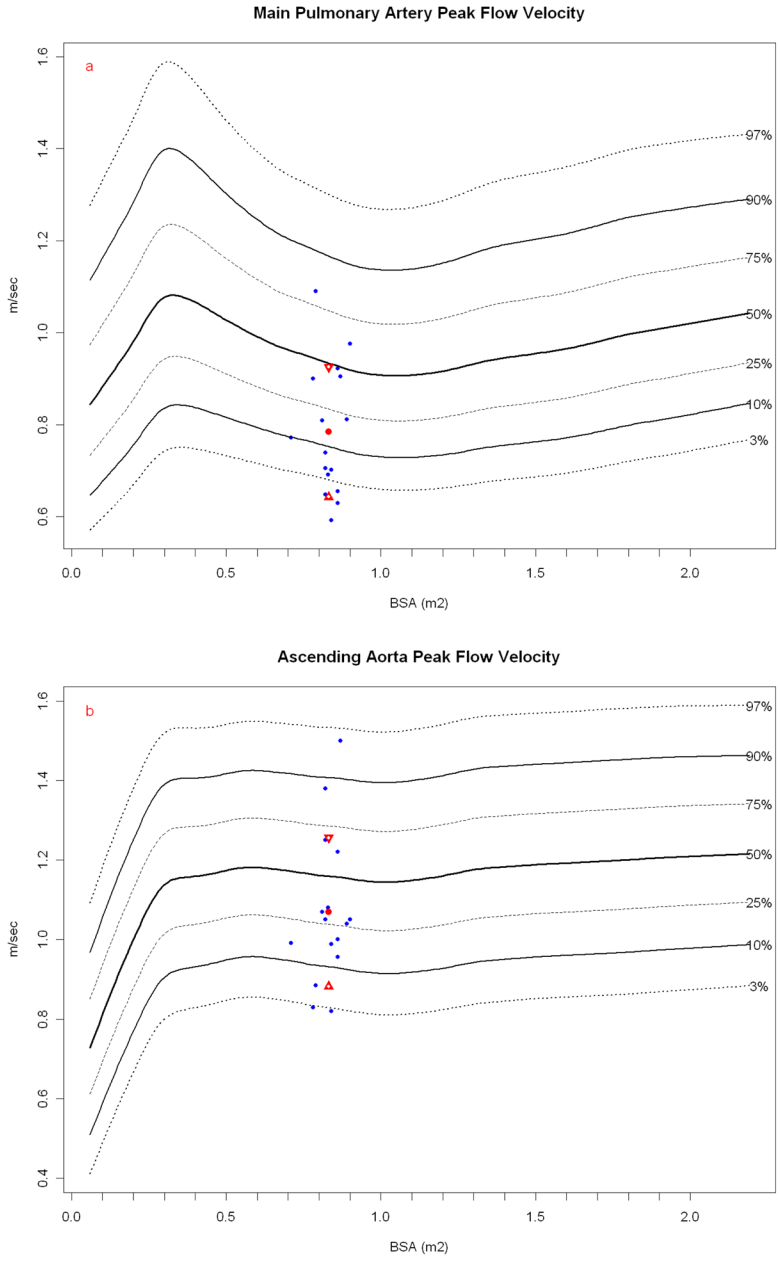

Figure 4.

Papio peak flow velocity (blue dots) in the (a) main PA and (b) ascending aorta plotted against resting human normals (ascending aorta, N = 13,284; PA, N = 13,634) obtained during resting transthoracic echocardiography with the *Papio* mean (red dot) and standard deviation (red triangles). *Papio* have similar flow velocities in the great arteries as humans, particularly considering these measurements are again done in anesthetized *Papio*.

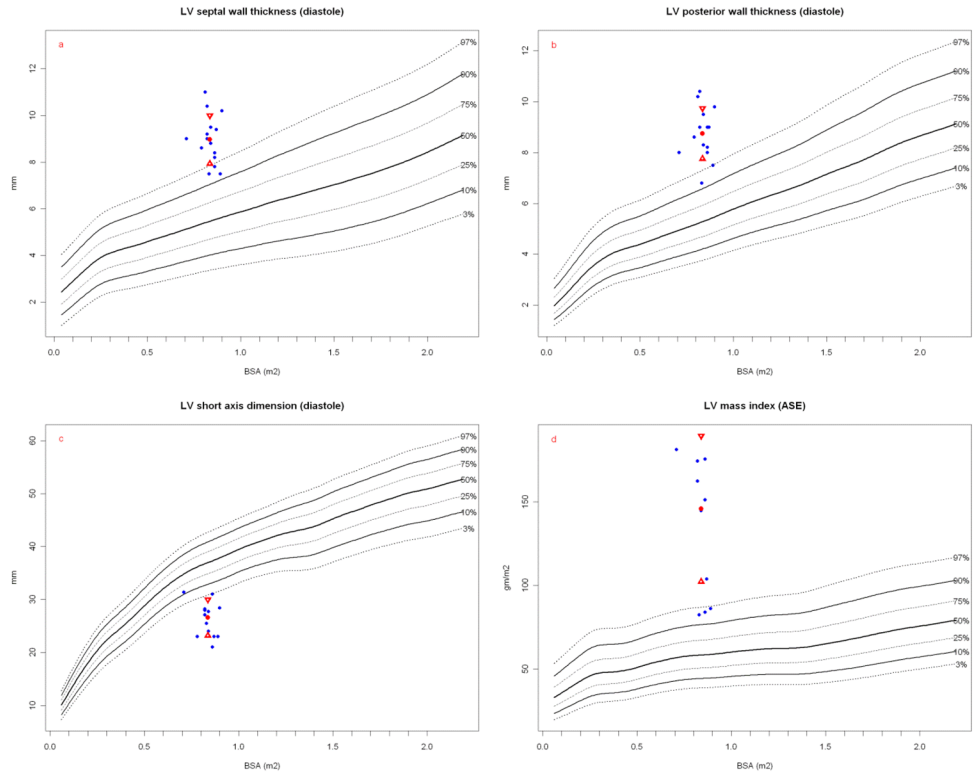

Figure 5.

LV wall thickness, short axis diastolic dimension, and calculated LV mass index. *Papio* measurements (blue dots) are plotted against a measured normal human cohort model. *Papio* mean (red dot) and standard deviation (red triangles) are shown. The number of normal human measurements used in the reference model is shown as "N=". (a) *Papio* LV septal wall thickness plotted on human normal model (N = 14,489) and (b) *Papio* LV posterior wall thickness plotted on human normal model (N = 14,486). Both wall measurements are significantly thicker than the normal range for humans of similar BSA. The *Papio* short axis diastolic chamber dimension (c) plotted on human normal model (N = 14,161) is significantly smaller than that predicted for humans of a similar height. The resulting calculated *Papio* LV mass indexed to body surface area (d) is significantly higher than the predicted normal range for humans of similar BSA. Calculated LV mass was obtained using the Troy formula [61] and then indexed to calculated BSA (all diameters are calculated in diastole):

$$\text{LV mass} = 1.05\left(\left[\text{LV internal diameter} + \text{posterior wall thickness} + \text{intraventricular septum thickness}\right)^3 - \left(\text{LV internal diameter}\right)^3\right])$$

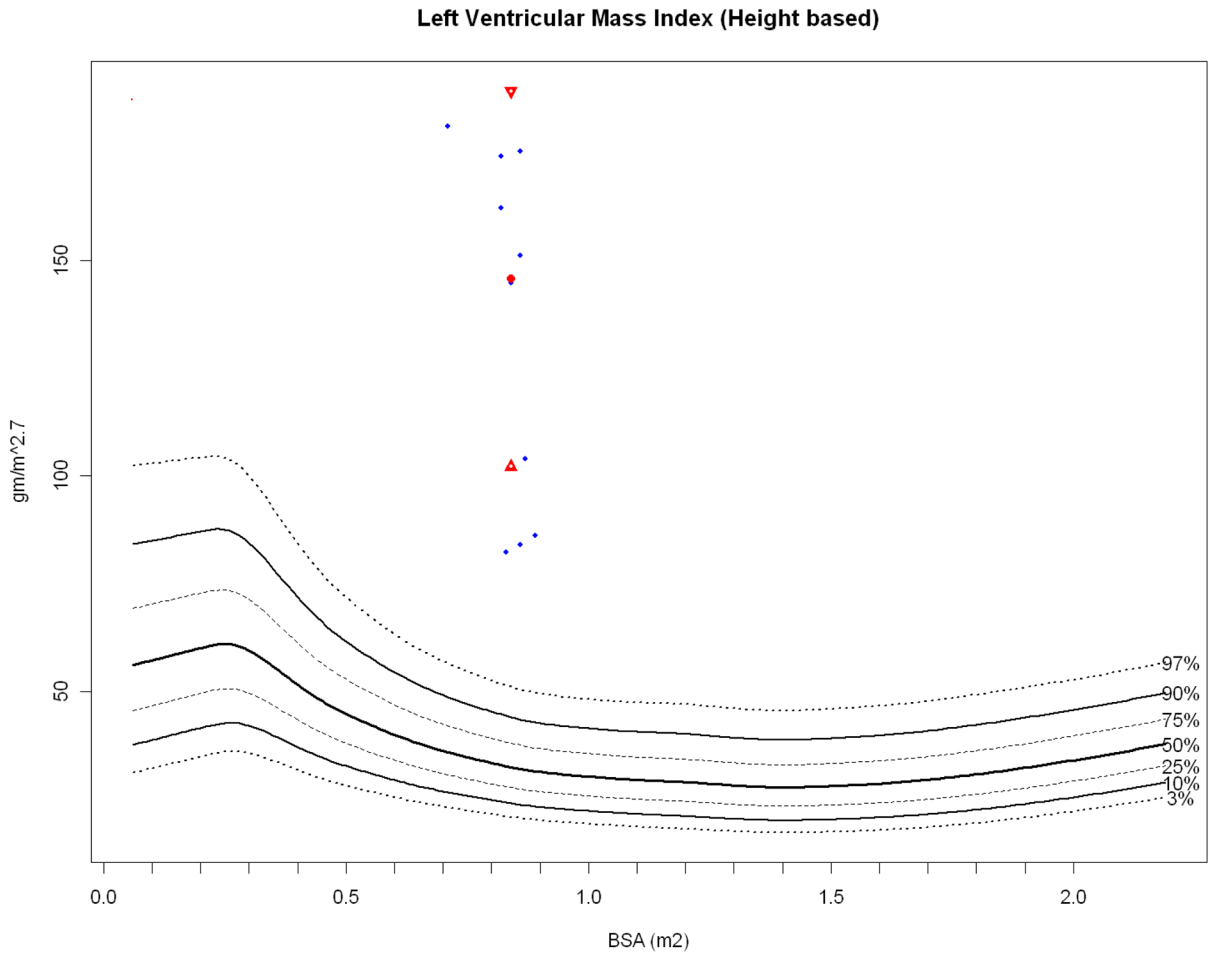

Figure 6.
LV mass index (height based). *Papio* height-based LV mass index (blue dots, ref below) plotted against height based human LV mass index (N = 13,941), with the Papio mean (red dot) and standard deviation (red triangles). *Papio* have significantly more LV myocardial mass than humans at similar height [51].

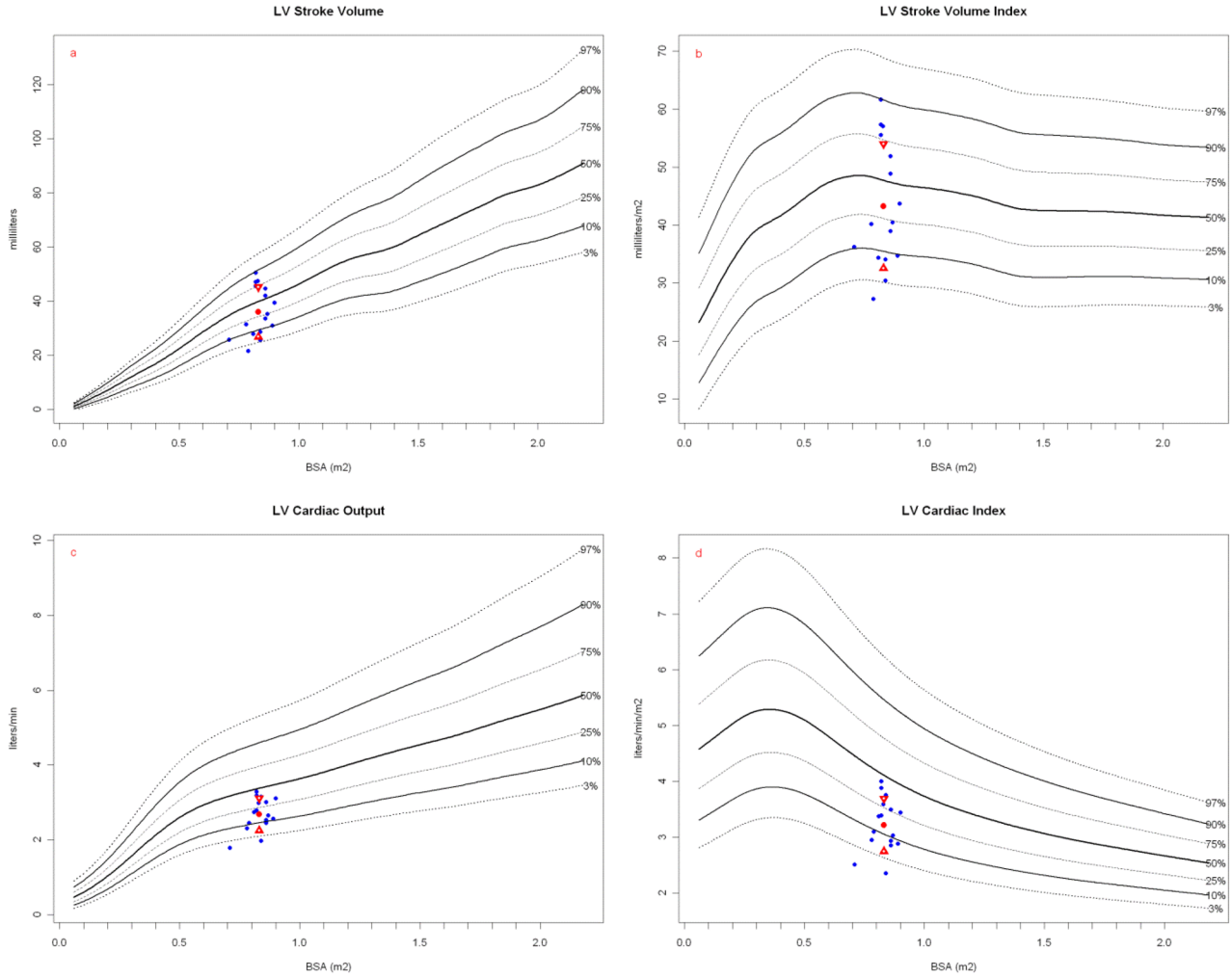

Figure 7.

LVSV and stroke index, LVCO and cardiac index. *Papio* measurements (blue dots) are plotted against a measured normal human cohort model. *Papio* mean (red dot) and standard deviation (red triangles) are shown. The number of normal human measurements used in the reference model is shown as "N=". (a) *Papio* LVSV plotted on human normal model and (b) *Papio* LVSV indexed to BSA plotted on human normal model (N = 14,013 for both). *Papio* LVCO (c) and cardiac index (d) are plotted on human normal model (N = 1,860 for both). *Papio* stroke volume was calculated using the Continuity Equation (see text), whereas the human stroke volume was calculated from m-mode measurements using the Teichholz method [53, 31]. Note that baboon "height" is measured as crown to rump length.

Table 1

The measured normative dimensional measurements via transesophageal echocardiography in young adult male baboons (*Papio hamadryas anubis*) as compared to literature values for adult human males [48, 30, 63, 40, 64, 60, 61, 35]. The median ± range for baboon normative dimensional measurements encompasses the 95% confidence interval.

Parameter, units	Baboon Normative Dimensional Measurements					Adult Human Normal Reference Values
	Median	Range	Min-Max	Mean	SEM	Range
BSA, m^2	0.83	0.2	0.70–0.90	0.83	0.01	0.6–2.5
RA, A-P diameter, cm	2.68	1.50	2.20–3.70	2.74	0.13	4.3–4.5
RA, M-L diameter, cm	2.46	1.40	1.96–3.36	2.52	0.12	3.3–3.7
RV cavity, Major axis, cm	3.90	1.60	3.20–4.80	3.96	0.12	6.7–7.5
RV cavity, Minor axis, cm	1.95	1.01	1.57–2.58	1.96	0.08	2.3–3.3
RV cavity free wall thickness, mm	4.50	1.40	4.00–5.40	4.63	0.11	4.0–5.0
RVOT diameter, cm	1.91	0.45	1.63–2.08	1.89	0.03	1.7–2.6
Tricuspid valve annulus, cm	2.30	0.50	1.95–2.45	2.27	0.04	2.0–4.0
PV annulus diameter, cm	1.70	0.34	1.50–1.84	1.70	0.04	1.7–2.7
[a] PV area, cm^2	2.11	1.28	1.48–2.76	2.15	0.09	2.2–3.4
PV area index, cm^2/m^2	2.43	1.44	1.87–3.32	2.60	0.10	1.8–3.1
Main PA diameter, cm	1.75	0.43	1.57–2.00	1.76	0.03	1.2–2.2
LA, A-P diameter, cm	3.15	1.60	2.40–4.00	3.07	0.11	2.0–5.2
LA, M-L diameter, cm	2.70	1.31	2.29–3.60	2.77	0.11	2.4–5.2
LV cavity, Major axis, cm	5.10	1.50	4.00–5.50	4.94	0.11	6.6–8.6
LV cavity, Minor axis, cm	2.71	1.04	2.10–3.14	2.66	0.08	4.2–5.9
LV cavity, septal wall thickness, mm	9.00	3.50	7.50–11.0	8.97	0.27	6.0–10.0
LV cavity, posterior wall thickness, mm	9.00	3.60	6.80–10.4	8.75	0.26	6.0–10.0
LVOT diameter, cm	1.72	0.46	1.59–2.05	1.75	0.03	1.5–2.3
MV annulus, cm	2.35	0.33	2.17–2.50	2.34	0.03	2.0–3.8
[a] MV area, cm^2	3.06	1.88	2.20–4.08	3.02	0.21	4.0–6.0
MV area (pressure half-time), cm^2	3.03	2.04	2.25–4.29	3.24	0.16	4.0–6.0
Aortic valve annulus, cm	1.60	0.38	1.42–1.80	1.60	0.03	1.8–2.5
Aortic valve area, planimetry, cm^2	1.85	0.94	1.60–2.54	1.96	0.07	2.3–4.0
[a] Aortic valve area, cm^2	1.84	1.13	1.32–2.45	1.90	0.08	2.3–4.0

Parameter, units	Baboon Normative Dimensional Measurements					Adult Human Normal Reference Values
	Median	Range	Min-Max	Mean	SEM	Range
Aortic valve area index, cm^2/m^2	2.34	1.43	1.52–2.95	2.31	0.09	1.7–2.2
Ascending aorta diameter, cm	1.80	0.52	1.44–1.96	1.74	0.04	2.1–3.4

[a] Calculated by the continuity equation

Prog Pediatr Cardiol. Author manuscript; available in PMC 2014 August 01.

Prog Pediatr Cardiol. Author manuscript; available in PMC 2014 August 01.

Table 2

Measured normative hemodynamic measurements via transesophageal echocardiography in anesthetized young adult male baboons (*Papio hamadryas anubis*) as compared to literature normal ranges for adult human males [48, 30, 63, 40, 64, 60, 61, 35]. The median ± range for baboon normative dimensional measurements encompasses the 95% confidence interval.

Parameter, units	Baboon Normative Measurements					Adult Human Normal Reference Values
	Median	Range	Min-Max	Mean	SEM	Range
Cardiac physiology, blood flow velocity (cm/sec)						
RVOT	58.50	31.30	43.50–74.80	58.59	1.74	40–75
Main PA	77.20	49.80	59.20–109.0	78.92	3.35	44–78
LVOT	78.80	53.30	48.70–102.0	78.43	3.46	70–110
Ascending aorta	104.0	68.00	82.00–150.0	106.3	4.43	72–120
Transmitral valve inflow, E-wave	59.40	36.30	43.20–79.50	59.84	2.68	60–130
Transmitral valve inflow, A-wave	24.30	33.00	16.00–49.00	27.28	2.13	E:A ratio = 0.75–1.50
Valve gradients (mmHg)						
Tricuspid valve, peak gradient	0.50	0.80	0.30–1.10	0.582	0.055	0.5–2.5
Tricuspid valve, mean gradient	0.30	0.40	0.10–0.50	0.294	0.029	0.5–0.8
PV, peak gradient	3.00	4.00	1.00–5.00	2.880	0.283	0.5–4.0
PV, mean gradient	1.00	2.00	1.00–3.00	1.590	0.173	0.1–3.0
MV, peak gradient	1.30	1.80	0.80–2.60	1.480	0.139	0.5–2.5
MV, mean gradient	0.60	0.70	0.30–1.00	0.653	0.069	0.3–2.0
AV, peak gradient	4.00	7.00	2.00–9.00	4.590	0.438	0.5–7.0
AV, mean gradient	2.00	4.00	1.00–5.00	2.530	0.244	1.0–5.0
Hemodynamics, units						
Heart rate, bpm	74.00	52.00	58.00–110.0	73.65	2.938	60–100
RVSV, mL	37.00	22.00	25.60–47.60	36.87	1.387	60–90
[a] RVCO, L/min	2.670	1.650	1.900–3.550	2.694	0.118	5.0–6.0
RV cardiac index, L/min/m^2	3.379	1.760	2.290–4.050	3.260	0.129	2.5–3.5
LVSV, mL	34.00	29.00	21.50–50.50	35.89	2.167	60–90
[a] LVCO, L/min	2.640	1.500	1.780–3.280	2.658	0.104	5.0–6.0
LV cardiac index, L/min/m^2	3.164	1.650	2.350–4.000	3.215	0.111	2.5–3.5

Parameter, units	Baboon Normative Measurements					Adult Human Normal Reference Values
	Median	Range	Min-Max	Mean	SEM	Range
LVEF, %	55.85	17.60	45.00–62.60	55.58	1.841	52–69
LV FAC, %	40.95	27.10	32.90–60.00	43.59	3.472	28–38

[a] Cardiac output calculated by the continuity equation

Table 3

Views of aortic valve (AV), pulmonary valve (PV), mitral valve (MV), tricuspid valve (TV), pulmonary artery (PA), left ventricle (LV), right ventricle (RV), LV outflow tract (LVOT) and RV outflow tract (RVOT) by transesophageal echocardiography (TEE) or transthoracic echocardiography (TTE) in baboons.

View	Acronym	Imaging Uses
Mid-esophageal short axis view of aortic valve	ME AVSAX[§]	Visualization of AV cusps in open and closed positions Measurement of AV area, effective orifice area
Mid-esophageal long axis view of aortic valve	ME AVLAX[§]	Visualization of LVOT, AV, ascending aorta Measurement of LVOT and AV annulus; estimation of AV regurgitation
Mid-esophageal inflow-outflow view of right ventricle (i.e. “wrap-around” view)	ME RVIO[§]	Visualization of RV inflow and outflow, TV and PV function Measurement of tricuspid and PV annulus diameters, main PA diameter
Mid-esophageal four-chamber view	ME4C[§]	Visualization of LV cavity (foreshortened), TV function Measurements of right and left atria, RV chamber, TV annulus diameter
Mid-esophageal two-chamber view	ME2C[§]	Visualization of left atrium, MV, LV Measurements of left atrium, MV, LV and MV pressure gradients
Mid-esophageal long axis view	ME LAX[§]	Visualization of the LV inflow and outflow; assessment of MV physiology
Mid-esophageal view of the right ventricle, two-chamber view	ME RV2C[§]	Visualization and measurements of right atrium and RV cavity (non-standard view)
Trans-gastric mid-papillary left ventricular short axis view	TG SAX[§]	Visualization of RV and LV; measurements of ventricular wall motion, LV volume, LV and RV wall thicknesses
Trans-gastric two-chamber view	TG2C[§]	Visualization of LV (long axis); measurements of LV wall thickness, cavity dimensions and ejection fraction
Trans-gastric long axis view	TGLAX[§]	Visualization of LVOT and AV with good alignment of blood flow across valve; measurement of AV pressure gradients and cardiac output
Upper-esophageal aortic arch short-axis view	UESAX[§]	Visualization of RVOT and PV with good alignment of blood flow across valve; measurement of PV pressure gradients and cardiac output
Left ventricular short axis view	LVSAX[†]	Evaluation of LV wall motion, wall thickness, measurement of fractional area change; imaging of RV; equivalent to TGSAX
Trans-thoracic apical long axis view	APLAX[†]	Good alignment of blood flow across AV; measurement of flow velocity in LVOT and across AV, quantification of AV gradients, valve area and LV cardiac output; analogous RVOT imaging can be achieved by slight rotation of probe to the right

[§]Transesophageal view (TEE)

[†]Transthoracic view (TTE)